

Reason from Context with Self-supervised Learning

Xiao Liu^{1,2}, Ankur Sikarwar^{1,2}, Gabriel Kreiman^{3,4}, Zenglin Shi^{1,2}, Mengmi Zhang^{1,2}

¹I²R and ²CFAR, Agency for Science, Technology and Research, Singapore,

³ Children’s Hospital, Harvard Medical School, USA, ⁴ Center for Brains, Minds, and Machines, USA

Address correspondence to mengmi@i2r.a-star.edu.sg

Abstract

Self-supervised learning (SSL) learns to capture discriminative visual features useful for knowledge transfers. To better accommodate the object-centric nature of current downstream tasks such as object recognition and detection, various methods have been proposed to suppress contextual biases or disentangle objects from contexts. Nevertheless, these methods may prove inadequate in situations where object identity needs to be reasoned from associated context, such as recognizing or inferring tiny or obscured objects. As an initial effort in the SSL literature, we investigate whether and how contextual associations can be enhanced for visual reasoning within SSL regimes, by (a) proposing a new Self-supervised method with external memories for Context Reasoning (SeCo), and (b) introducing two new downstream tasks, lift-the-flap and object priming, addressing the problems of “what” and “where” in context reasoning. In both tasks, SeCo outperformed all state-of-the-art (SOTA) SSL methods by a significant margin. Our network analysis revealed that the proposed external memory in SeCo learns to store prior contextual knowledge, facilitating target identity inference in the lift-the-flap task. Moreover, we conducted psychophysics experiments and introduced a Human benchmark in Object Priming dataset (HOP). Our results demonstrate that SeCo exhibits human-like behaviors.

1. Introduction

Self-supervised learning (SSL) aims to learn discriminative visual representations from unlabeled images, which could be transferred to downstream tasks such as object recognition (Fig. 1a) and object detection (Fig. 1b). Recent works [47, 40] find out that mitigating contextual biases, caused by co-occurrences of objects and context in a complex scene, would improve the generalization ability of SSL to these downstream tasks. However, these object-centric methods would potentially

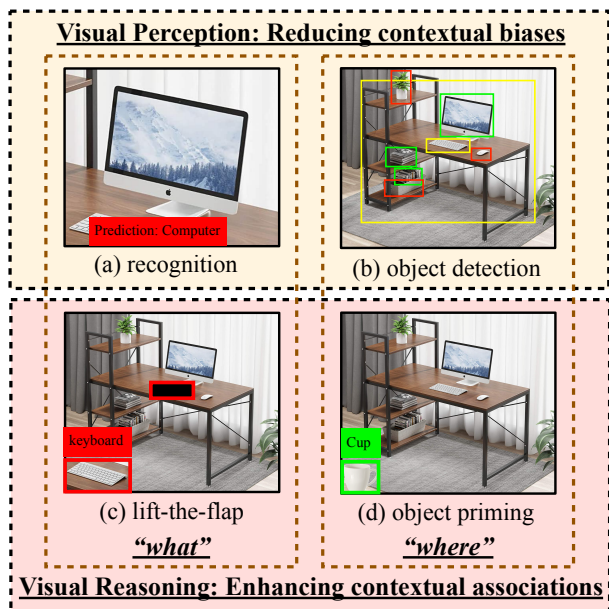


Figure 1. Schematic illustration of “what” and “where” problems of perception and reasoning via self-supervised training on natural images. In parallel to standard perception tasks in object recognition (a) and detection (b), two protocols are introduced to evaluate contextual reasoning ability: (c) Lift-the-flap task and (d) Object priming task. In (c), the task is to reason about the scene context and infer what a target object hidden behind a flap (black patch) is in a natural image. The original image (bottom left) reveals the target object (“keyboard”) which was not shown in the actual experiments. In (d), the task is to decide where to put the given object in the scene, e.g. to put the cup (at the bottom left) in the study room scene.

de-associate the objects and contexts and thus fail to address scenarios where contextual information is crucial, such as recognizing/inferring small, blurred, or occluded distant objects (Fig. 1c). Objects and contexts always come as pairs in a nature scene. In this light, humans are adept at exploiting contextual cues to fill in information gaps in their sensory input. For example, in Fig. 1c, based on

the scene context, one can infer that the hidden object on the table can be a keyboard or a book but never a car. To date, context reasoning capacity has been studied with supervised learning methods [60, 3], while there is a lack of counterpart in SSL literature. Therefore, in this paper, we delve into the question of whether and how contextual associations can be enhanced for visual reasoning in a self-supervised manner.

To bridge the above gaps, we propose a **Self-Supervised Learning Method for Context Reasoning (SeCo)**, where the pre-training objective is to learn to associate objects and their contexts in the embedding space. Briefly, SeCo first uses unsupervised methods to discover region proposals containing potential target objects of interest. Next, the target object of interest and its surrounding context is processed separately by two independent image encoders. Humans rely on prior knowledge of various objects and their mutual relationships to establish contextual associations. Inspired by it, we introduced a learnable external memory to store learned contextual priors.

As an initial effort in this direction, we established a framework to utilize contextual knowledge for context-aware SSL. Given unlabeled images containing multiple objects in natural scenes, the objective of context-aware SSL is to learn object-context associations. To showcase the use of context in practical applications, such as tiny object recognition and placing items in context-appropriate locations for assistive robots, and to evaluate the context reasoning capabilities of all computational models, we introduced two evaluation protocols, lift-the-flap and object priming, addressing the problems of “what” and “where” in context reasoning. Specifically, the lift-the-flap task (**Fig. 1e**) requires all the models to utilize the scene context to infer the class of the hidden target object behind a flap (a given black patch). In the object priming task (**Fig. 1d**), given an image and a target object (not already present in the image), models are expected to predict contextually correct image regions for placing the target object.

We stress-tested SeCo and SOTA SSL methods on in- and out-of-domain test sets of three datasets in lift-the-flap and object priming tasks. SeCo achieved remarkable performance and beats SOTA SSL methods in all the experiments. To benchmark the model performance in object priming, we conducted human psychophysics experiments. Our results suggest that SeCo exhibits human-like behaviors. Moreover, We gain insights into the role of our external memory from intensive network analysis. We summarize our key contributions below:

- We are the first work to investigate whether and how contextual associations can be enhanced within the SSL regime. We established a new framework for the SSL community to study context reasoning,

where lift-the-flap and object priming protocols are introduced to benchmark the contextual reasoning ability of SSL methods.

- We proposed a simple yet effective SSL method (SeCo) to learn contextual associations. SeCo beats SOTA SSL methods by a large margin on in-domain and out-of-domain test sets of three datasets in lift-the-flap and object priming tasks.
- We contributed a new object priming dataset (HOP) and human benchmarks on HOP with psychophysics experiments. Our SeCo achieves human-level performance and exhibits human-like behaviors.

2. Related Work

Given that ground truth labels are costly to obtain for supervised learning, SSL has become an emerging trend in ML. Past handcrafted pretext tasks have been designed to improve the quality of learned scene representations such as “inpainting” the randomly masked regions of an image [42, 33, 43, 44]. Another group of works [28, 58, 39, 26, 9, 56] use contrastive learning techniques for SSL by pulling positive samples together and pushing negative samples away. However, mining negative examples is not always feasible; thus, current research has shifted focus to representation learning solely from positive samples [11, 24, 50, 59, 1, 7]. With the success of transformer-based models in NLP and vision tasks [18], there has also been a trend in SSL of reconstructing images from randomly masked image patches [25, 10]. However, all these previous methods focus on learning image-level representations from monotonously large, salient, and centered objects [14]. They often fail to capture instance-level associations in the scene. Unlike all these works, our SeCo is capable of learning object-context associations from complex images where there could be multiple objects in the scene.

Several SSL methods [6, 34] use external memories to store trainable object prototypes and use them to assign similar images to distinct clusters. In contrast to these methods, our external memory stores prior knowledge on object-context associations so that our SeCo can flexibly retrieve useful object information from context cues in the visual scenes.

The context of a scene [51, 29, 16, 35, 17] is crucial to computer vision tasks, such as object recognition [60, 3], place recognition [54], object detection [37, 12], semantic segmentation [41], and visual question answering [48]. Supervised learning methods based on statistical optimization tools [22, 57, 32, 8], graph neural networks [2, 13, 15, 30], and transformers [5, 3] are proposed to learn contextual knowledge. However, numerous works [46, 47, 40] found that models suffer from contextual biases caused by co-occurrences and try to improve the object-centric generalization ability by removing such biases. Breaking

away from these works, we investigated the problem of whether and how to leverage contextual cues in the SSL setting. Although previous works introduced datasets with context variations, such as ImageNet-9 [55], these datasets often contain very few objects, discarding the useful information of object co-occurrences in complex scenes. As we aim to study context reasoning abilities in “what” and “where” problems, we introduce lift-the-flap and object priming protocols, focusing on datasets with multiple objects and rich context [4].

3. Method

We propose a Self-Supervised Learning Method for Context Reasoning (SeCo) which learns associations between objects and their contexts in natural images (Fig. 2). SeCo consists of three components: (a) target discovery module, (b) two-stream visual processor, and (c) external memory. First, the target discovery module uses unsupervised region proposal methods to locate potential objects of interest on the full image I_f . Each region proposal together with the full image I_f is subsequently converted to pairs of target images I_t and context images I_c (Sec. 3.1). Second, the two-stream visual processor consists of two independent pairs of CNN encoders and projectors, extracting information from I_t and I_c respectively (Sec. 3.2). Third, SeCo employs a trainable external memory (Sec. 3.3) to store knowledge priors about target-context associations learned during the training phase (Sec. 3.4). Features from I_c serve as queries to retrieve context-relevant prior knowledge from the external memory with an attention mechanism. The retrieved information provides the complementary signal to the context stream and gets compared with the target features from I_t of the object stream to maximize the agreement between the stored prior knowledge and the context-relevant object in the embedding space. Refer to **Supp.** for the PyTorch-style pseudocode of SeCo’s training algorithm.

3.1. Context-Object Pair Discovery

Objects play an important role in context reasoning [19]. To learn object-object and object-context associations, we propose a context-object pair discovery module to exploit regions containing objects of interest.

We adopt the selective search algorithm [52] to generate regions of interest (RoI) that potentially contain objects. It is worth noting that selective search is an unsupervised learning algorithm. It performs heuristic searches on hundreds of anchor boxes and proposes RoIs by hierarchically grouping similar regions based on color, texture, size, and shape compatibility. To reduce false positives among many RoIs, we filter out resultant regions according to their area ratio (with a maximum of 0.1) and aspect ratio (within 0.2 and 5). Moreover, we merge

RoIs with heavy overlaps by setting the threshold of IoU(intersection over union) as 0.3. For each selected RoI, we generate a pair of target images I_t and context image I_c . I_t is cropped out of full image I_f . The entire image with the RoI blacked out with zeros forms the context image I_c .

3.2. Feature Extraction with CNN

Due to the eccentricity dependence, human vision has the highest acuity at the fovea and the resolution drops sharply in the far periphery with increasing eccentricity. For example, while we are fixating on the mug on the table, the mug is often perceived in high resolution while the context gist of the kitchen scene is processed at low resolution in the periphery. Seeking inspiration from this, we propose a two-stream visual processor, with one object stream dedicated to encoding the target image I_t and the other context stream dedicated to encoding the context image I_c . The encoded representations are denoted as $h_c = E_c(I_c)$ and $h_t = E_t(I_t)$, where $E_t(\cdot)$ and $E_c(\cdot)$ are target and context encoders and h_t and $h_c \in \mathbb{R}^D$. Since the features useful for reasoning and perception are different, we do not enforce weights sharing between the encoders. We demonstrate its benefit in Sec. 5.3.

3.3. Training With An External Memory

As suggested by cognitive and neuroscience works [60, 45, 49], context processing often happens very fast in the brains. The perceived scene gist serves as queries to retrieve prior knowledge from the semantic memory to module object recognition in a top-down manner. To mimic this underlying mechanism of context modulation in the biological brains, we introduce an external memory with trainable parameters, accumulating prior knowledge of context-object associations. Here, we introduce math notations and formulations of our memory mechanism. Different from the well-established cross-attention mechanism [53], the objectives of our external memory focus on dynamically retrieving and updating the prior knowledge.

We define the external memory as a 2D matrix with trainable parameters, which consists of K memory slots of H dimension, denoted as $M = \{m_1, \dots, m_K\}$, $M \in \mathbb{R}^{H \times K}$. Each memory slot is associated with a key, where $\phi_k(\cdot) : \mathbb{R}^H \rightarrow \mathbb{R}^H$ defines the linear mapping from the memory content to the keys $\phi_k(M)$. The encoded representation h_c from the context stream serves as queries to the external memory after a linear projection operation $\phi_c(\cdot) : \mathbb{R}^D \rightarrow \mathbb{R}^H$. The retrieved prior knowledge $s_c \in \mathbb{R}^H$ from M can then be represented as

$$s_c = \text{SOFTMAX}\left(\frac{\phi_c(h_c)\phi_k(M)^T}{\sqrt{H}}\right)M \quad (1)$$

where $\text{SOFTMAX}(\cdot)$ is the standard softmax operation.

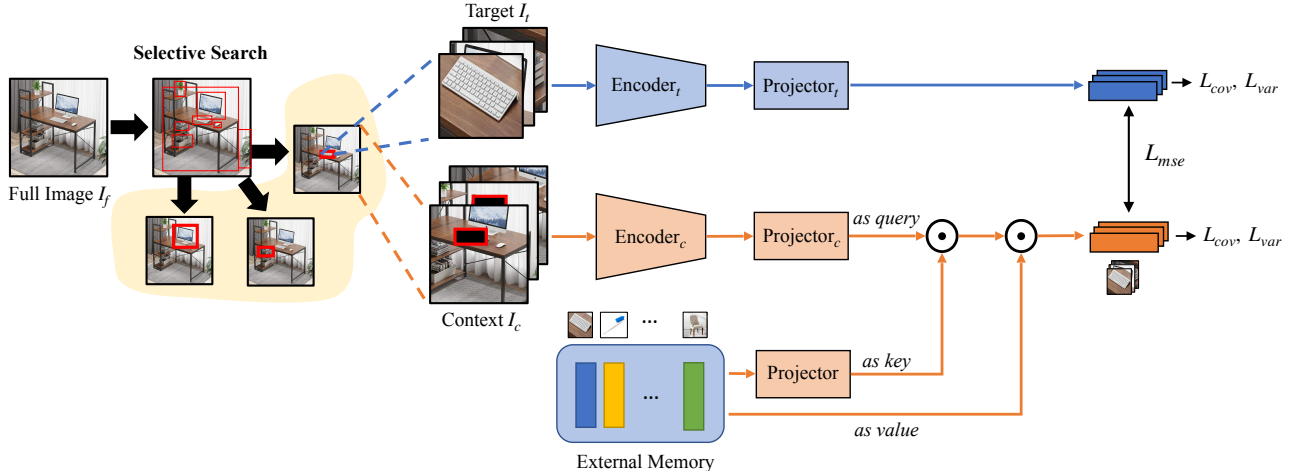


Figure 2. **The architecture overview of our Self-supervised learning for Context reasoning (SeCo).** The architecture is comprised of three components: target discovery module, two-stream visual processor, and external memory. SeCo uses an unsupervised method to discover potential targets. The discovered targets are then converted to multiple context-object pairs (Sec. 3.1). SeCo leverages non-shared networks to encode targets and contexts separately (Sec. 3.2). In addition, SeCo uses a trainable external memory to store the contextual priors learned during the training phase, which can then be used as a complementary signal during inference (Sec. 3.3). Finally, we use a joint loss which maximizes agreement between target and context with L_{mse} in the embedding space and regularizes the learned representations with L_{cov} and L_{var} , increasing diversity (Sec. 3.4).

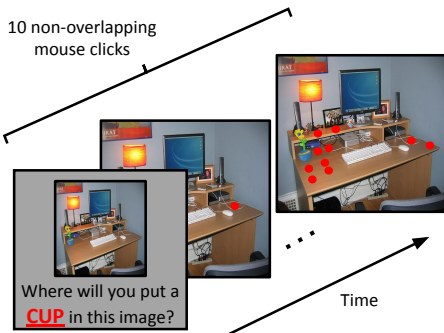


Figure 3. **Schematic for human psychophysics experiments in object priming task.** Subjects were presented with a natural image with a target object and were to put the object at appropriate locations by making 10 non-overlapping mouse clicks (red dots).

3.4. Loss Components

To encourage M to learn rich and meaningful context-object associations, we introduce three types of losses. Ideally, given only the scene gist, the retrieved prior s_c from M should represent useful object information related to the given context (i.e. “what could be the target object given the scene gist” versus “the actual object seen in the scene”). Thus, we apply a mean squared error loss l_{mse} to maximize the agreement between s_c and h_t . To make the vector dimension comparable, h_t is projected to $s_t \in \mathbb{R}^H$ in the embedding space via $\phi_t(\cdot)$.

As shown by previous works in non-contrastive learning [1, 11], maximizing the agreement between two-stream visual processors alone may lead to model collapses.

For example, external memory stores and outputs trivial knowledge of all zeros, while the visual processor encodes images to representations of all zeros. In this case, s_c and s_t align perfectly, but encoded object representations and content in M are meaningless.

Thus, to prevent model collapses, we follow [1] to enforce covariance L_{cov} and variance L_{var} regularization on both object and context streams. L_{var} maintains the variance of batch data sample representations, encouraging object class diversities, while L_{cov} de-correlates channel-wise variables to diversify attributes of an embedding, i.e. maximize independent attributes to represent objects. SeCo is jointly trained with the total loss:

$$L_{total} = \alpha L_{mse}(s_c, s_t) + \beta [L_{var}(s_c) + L_{var}(s_t)] + \gamma [L_{cov}(s_c) + L_{cov}(s_t)] \quad (2)$$

where $\alpha = 25$, $\beta = 25$ and $\gamma = 1$ are hyper-parameters weighting different loss components (see **Supp.** for the hyper-parameter analysis).

3.5. Implementation Details

Augmentations. Data augmentation techniques are widely used at image levels in SSL. We applied standard image augmentations on both I_t and I_c , including color jitter, grayscale, horizontal flip, gaussian blur, and color normalization. Moreover, the random resized crop is another effective technique in SSL. However, directly applying this approach is not feasible in our case. Thus, we extended the standard approach to context-object image

pairs with context-aware crops by ensuring that the relative locations among objects are preserved and the bounding box encompassing the target object is always intact and present on I_c after geometric transformations.

Network architecture. We use ResNet-50 [27] with $D = 2048$ output units as our encoders. We set the size of M as $K \times H = 200 \times 512$ and initialize M by the Xavier uniform initializer [21]. We demonstrate the benefit of the external memory and vary its sizes in the ablation study (Sec. 5.3).

Training. We set the base learning rate to $lr = 0.2 * \text{batch_size}/256$ [23]. The learning rate grows linearly from 0 to base value during the first 10 epochs and then decays with a cosine scheduler [38] for the rest of epochs with a minimum value of 0.0002. All our source codes and data will be publicly available.

4. Experiments

4.1. Datasets

COCO-Stuff Dataset [4] contains 160K natural images from MSCOCO [36] with 80 thing classes and 91 stuff classes in total. Importantly, this dataset captures complex relationships between multiple objects and their contexts.

PASCAL VOC07 Dataset [20] contains 9,963 images of realistic scenes with a total of 20 object classes.

Out-of-Context Dataset (OCD) [3] contains 15,773 synthetic test images of indoor scenes with 36 classes under 6 different contextual conditions. In our work, we only consider *normal context* condition with 2,309 test images.

To evaluate whether the learned contextual knowledge from SSL methods can generalize well in out-of-domain settings, we come up with two custom regimes on pretext training, fine-tuning, and testing:

COCO-VOC contains those images from COCO-Stuff where the object classes present in the scene overlap with the object classes from the PASCAL VOC07 dataset. Overall, 20 classes overlap between COCO-Stuff and PASCAL VOC07 datasets. Refer to the **Supp.** for the list of selected 20 classes. We used the training set of COCO-VOC for pre-training and fine-tuning and then tested all the models on the test set of COCO-VOC (in-domain) and PASCAL VOC07 dataset (out-of-domain).

COCO-OCD includes those images from COCO-Stuff where the object classes in the scene overlap with the object classes from the OCD dataset. Here, in total 15 classes overlap between COCO-Stuff and OCD datasets. Refer to the **Supp.** for the list of selected 15 classes. We used the training set of COCO-OCD for pre-training and fine-tuning and then tested all the models on the test set of COCO-OCD (in-domain) and OCD dataset (out-of-domain).

4.2. Baselines

We compare our SeCo against a list of SSL methods including Context Encoder[44], SimCLR[9], SimSiam[11], DINO[7], and VICReg[1]. For all the methods, we use standard ResNet-50 backbones, with weights pre-trained on ImageNet obtained from their own public checkpoints. We used the initial implementations from their original papers. For Context Encoder, since it was originally trained with AlexNet [31], we re-implement it with the standard ResNet-50 backbone. In addition to all the SSL baselines, we include a supervised learning baseline that takes I_c as inputs, given the ground truth target labels. See **Supp.** for further details.

4.3. Evaluation Protocols for Context Reasoning

Lift-the-Flap. We introduce the lift-the-flap task to address the problem of “what” in context reasoning. In the task, all models are required to rely only on context information to infer the class identity of the hidden target object. To adapt the pre-trained model to this task, we freeze the model weights for feature extraction and then only train a linear classifier to predict the hidden target object. We report the performance in Top-1 accuracy of all methods in **Tab. 1**.

Object Priming. We introduce the object priming task to address the problem of “where” in context reasoning. Specifically, the model is given an image and a target object as inputs and has to predict contextually correct locations for placing the target object. As there was no object priming dataset in the literature, we curated our own dataset.

[Stimulus designs] We curated semantically relevant 864 unique image-object pairs on 206 images from the test set of MSCOCO-OCD dataset (Sec. 4.1). Eggs tend to be nearby other eggs. To avoid this “crowding” effect that could bias humans and models in placing the same target objects in the same locations, for each image-object pair in object priming, we made sure that there are no object instances present on the context image whereby these object instances belong to the same class as the given target object. See **Supp.** for details about selecting these image-object pairs.

[Human response collection] We followed standard Institutional Review Board protocols and used Amazon Mechanical Turk (AMT) to collect responses from a total of 437 human subjects. For each subject, we randomly sample 20 image-object pairs and present the 800×800 image along with the question “Where would you put this $[obj]$?” where $[obj]$ corresponds to the sampled target object. The subjects are required to make non-repeated 10 mouse clicks at relevant regions of the given image. For each image-object pair, we collect responses from exactly 3 human subjects which gives us 30 unique clicks in total per image-object pair. We show the schematic for the human psychophysics experiment in **Fig. 3** (see **Supp.** for AMT interface). For each image, we consolidated all 30 click coordinates and

	Method	In Domain	Out Of Domain
COCO-VOC	<i>Supervised</i>	48.59	53.69
	Context Encoder [44]	15.78	14.82
	SimCLR [9]	32.78	37.65
	SimSiam [11]	39.79	45.76
	DINO [7]	42.06	48.07
	VICReg [1]	44.89	52.58
	SeCo (Ours)	52.31	57.27
COCO-OCD	<i>Supervised</i>	42.51	20.17
	Context Encoder [44]	20.55	10.68
	SimCLR [9]	35.78	15.51
	SimSiam [11]	42.46	19.36
	DINO [7]	43.21	15.34
	VICReg [1]	44.34	24.31
	SeCo (Ours)	52.43	31.37

Table 1. **SeCo outperforms all baselines in lift-the-flap task.** We test all the baselines (Sec. 4.2) on in-domain and out-of-domain images over 3 datasets (Sec. 4.1) and report top-1 accuracy averaged over 5 runs (Sec. 4.3).

generated the click probabilistic map of size 25×25 . After several post-processing steps (see Supp.), we produce final human priming maps (Column 2 of Fig. 4).

[Model-human comparisons] To predict priming maps for all the models, we converted the object priming task to a series of lift-the-flap tasks with the following steps: (1) we divide the context image into patches. (2) We covered a single image patch with a flap (black pixels) while the remaining patches remain intact. (3) We tested all models fine-tuned on COCO-OCD from the lift-the-flap task in (2) and recorded the predicted classification probability of the model for the given target object class in the object priming task. (4) We iterated through (2) and (3) until we exhaustively performed “lift-the-flap” tasks over all the image patches. (5) For each image patch, we then have a classification score indicating how confidently the model would put the given target object in that patch. We consolidated all the probabilities for all the patches and generated the priming map for each model. As the model predictions were sensitive to the patch sizes, we varied the patch sizes and normalized the final priming map over all patch sizes (see Supp. for details). We compare the similarity between human priming maps and the priming maps generated by all models using root-mean-squared errors (RMSE) and reported the results in Tab. 3.

5. Results

5.1. Lift-the-flap task

We report the top-1 target inference accuracy of all models in the lift-the-flap task (Tab. 1). SeCo achieves an overall accuracy of 52.31% and 52.43% on the test sets of COCO-VOC and COCO-OCD, surpassing all the baselines by a large margin. Context Encoder [44] is trained with the hand-crafted pretext task by reconstructing the masked region at the pixel level. However, its performance

Object Stream	Context Stream	Accuracy
SimCLR	-	55.38
SimCLR	SimCLR	57.33
SimCLR	SeCo	58.29
SimSiam	-	67.12
SimSiam	SimSiam	70.93
SimSiam	SeCo	70.72
DINO	-	70.84
DINO	DINO	73.35
DINO	SeCo	74.17
VICReg	-	74.52
VICReg	VICReg	75.53
VICReg	SeCo	76.46

Table 2. **SeCo enhances object recognition abilities of all baselines.** We report top-1 accuracy averaged over 5 runs on COCO-OCD dataset in object recognition tasks under three conditions: (1) without contextual priors; (2) with contextual priors predicted by the baselines themselves and (3) by our SeCo.

is inferior to other baselines and our SeCo, implying that pixel-level reconstruction focuses on details of visual features, discarding the local contextual associations, such as object co-occurrences. Next, we observed that contrastive methods like SimCLR [9] performed worse compared with non-contrastive methods like SimSiam [11], DINO [7], and VICReg [1]. It suggests that multiple objects could co-occur in the same context and making a selection of negative samples is non-trivial and challenging in context-aware SSL. Moreover, we noted that SeCo even surpasses the supervised learning baseline, suggesting that SeCo learns to capture meaningful contextual associations in the scenes, beneficial for downstream reasoning tasks.

A bird flies in the sky regardless of whether the scene is depicted in Picasso or Monet styles. Contextual associations should be invariant to domain shifts of visual features. We test all models in out-of-domain datasets, PASCAL VOC07 and OCD. SeCo outperforms previous approaches on out-of-domain images, with top-1 accuracy of 57.27% and 31.37% on PASCAL VOC07 and OCD, respectively. Compared across domains, we noted that all methods achieve slightly better performance in PASCAL VOC07 than COCO-VOC, because both COCO-VOC and PASCAL VOC07 contain natural images, and the context-associated object pairs on these images are more prevalent on VOC. On the contrary, when the domain shifts from natural images in COCO-OCD to synthetic images in OCD, we saw a big performance drop for all the models. Yet, our model gets less impaired due to domain shifts, highlighting that our SeCo learns context associations rather than correlations of visual features.

One benefit of the lift-the-flap task is to identify small, blurred, or occluded distant objects. To demonstrate this point, all the baseline SSL methods leverage contextual information in the lift-the-flap task as priors to modulate their predicted probability distribution in the object

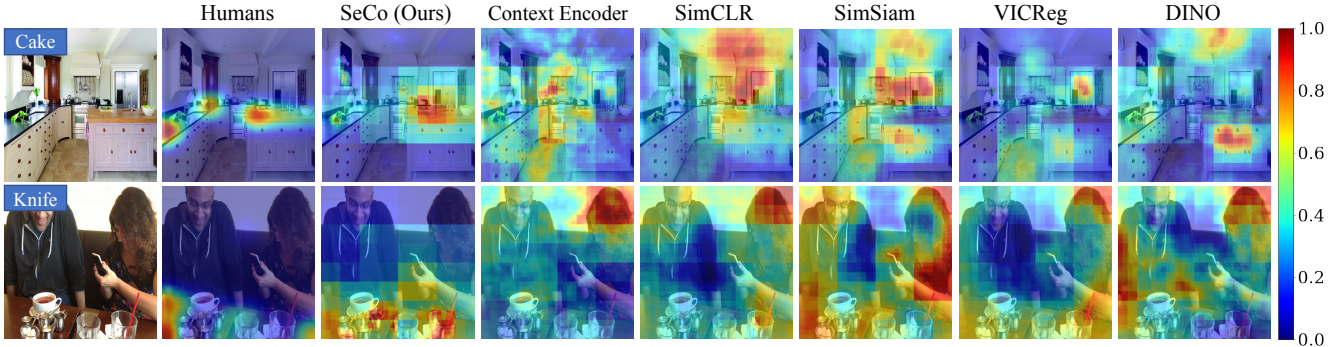


Figure 4. **SeCo priming maps highlight contextually relevant regions of the image and closely approximate human choices in the object priming task.** The leftmost column shows the input image and the given target object class label used for priming. The rest of the columns from left to right are priming maps from humans, predicted by our SeCo and predicted by all baselines (Sec. 4.2).

Method	RMSE
<i>Supervised</i>	0.37 ± 0.07
Human Agreement	0.17 ± 0.05
Context Encoder [44]	0.41 ± 0.06
SimCLR [9]	0.44 ± 0.07
SimSiam [11]	0.43 ± 0.09
DINO [7]	0.42 ± 0.07
VICReg [1]	0.40 ± 0.09
SeCo (Ours)	0.32 ± 0.06

Table 3. **Root mean square error (RMSE) between human priming maps and maps predicted by computational models in object priming task.** Lower is better. Error bars show the standard deviation calculated across samples. RMSE for the human agreement was calculated by comparing priming maps across the 3 human subjects for individual image-object pairs.

recognition task on COCO-OCD dataset. See **Supp.** for implementation details. We report the top-1 recognition accuracy in **Tab. 2**. Compared to the case when all SSL baselines recognize objects based on I_t alone, we observe higher top-1 accuracy after incorporating context. This suggests that context enhances object recognition. Moreover, after substituting the prior distribution predicted by all SSL baselines themselves in the lift-the-flap tasks with our SeCo, we saw another significant boost in object recognition accuracy. This emphasizes the superiority in the context reasoning ability of our SeCo against all SSL baselines. Consistent with previous works [60, 3], we also break down the results according to the target object sizes and we find that the effect of contextual cues is more prominent in recognizing smaller target objects (see **Supp.** for results and more analysis).

5.2. Object priming task

We compare human priming maps with the maps predicted by all models and report RMSE scores in **Tab. 3**. As an upper bound, we calculated the between-human RMSE score (0.17) by comparing maps from pairs of humans. SeCo achieves the lowest RMSE of 0.32 compared

	Discovery	NSA	Memory	Accuracy
I	SS	✓	✓	52.43
II	GT	✓	✓	49.61
III	RG	✓	✓	36.95
IV	Standard	✓	✓	43.01
V	GT	✗	✓	37.48
VI	GT	✓	✗	44.07

Table 4. **Ablation Study.** Top-1 accuracy in lift-the-flap on COCO-OCD for ablated models is reported. See **Sec. 5.3** for ablation descriptions. Default settings of SeCo are **highlighted**.

to all baselines, emphasizing that SeCo predicts more human-like priming maps than all the baselines. In general, we also noticed that there still exists a big gap between model and human agreements in object priming. This inferior performance could be explained away by three reasons: (1) models are not finetuned on the HOP dataset; (2) discrete priming maps have different-sized grids from the ones used in human experiments; and (3) it is still challenging for machines to capture how humans incorporate context, who already have decades of daily experience with context.

To assess the quality of the predicted priming maps by all models, we also visually examined qualitative examples (**Fig. 4**). In contrast to all the baselines which tend to generate relatively uniform flat priming maps, our SeCo manages to predict semantically reasonable locations to place the target objects. Note that we do not train or fine-tune any methods to fit human priming maps. It is quite remarkable that our SeCo can transfer the knowledge in context-object associations to infer target-relevant semantically-correct locations in the scene.

5.3. Ablation and memory analysis

We assessed the importance of design choices by training and testing ablated versions of SeCo on COCO-OCD.

First, to demonstrate the effectiveness of the object discovery module, we replaced the object-context image

pairs proposed by selective search [52] with randomly generated object-context image pairs (Tab. 4, III, RG). As expected, RG acts as the lower bound of the discovery module, and the top-1 accuracy drops by 16%. This highlights that the “objectiveness” in generated regions helps learn contextual associations. We also trained SeCo on the object-context image pairs from annotated ground truth bounding boxes (Tab. 4, II). Surprisingly, SeCo performs better with SS by 3%. It is possible that the exploited RoIs by the selective search contain small objects which are hardly labeled by human annotators but are useful for context-aware SSL. Next, to further stress-test that our external memory dedicates to storing context-object associations, rather than a general form of “inpainting” buffer for filling in any missing pixels on I_c , we substituted I_c and I_t with two standard augmented views of the full image I_f (Tab. 4, IV). The inferior performance to our SeCo highlights: (1) context-object pair discovery module is essential, and (2) augmented memories work best in reasoning on object identity from context.

Next, we trained two separate encoders $E_t(\cdot)$ and $E_c(\cdot)$ in SeCo (Sec. 3.2). Here, we enforced weight-sharing encoders (Tab. 4, V). SA achieved a lower top-1 accuracy than SeCo, suggesting that the same features for both target and context streams are insufficient to reason about context.

To study the effect of the external memory in context reasoning, we remove the external memory from our default SeCo (Tab. 4, VI). The performance of the model without memory drops by around 5%, demonstrating that the external memory enhances the reasoning ability of SeCo. We also vary the number of memory slots from 100 to 800 (see Supp. for the results). There is a moderately positive increase of 2.5% in Top-1 accuracy in lift-the-flap. However, we observed a non-monotonic trend in Top-1 accuracy, when we vary the feature dimension of the external memory (see Supp. for the results). The top-1 accuracy peaks when the feature dimension equals 512. It suggests that larger memory capacity in general helps learn and store richer context-object associations; however, an overly large-sized memory may hurt context reasoning abilities, as the memory fails to generalize the learned contextual knowledge due to over-fitting.

We further probe what the external memory has learned by visualizing the pairwise KL divergence of attention score over memory slots for object categories in COCO-VOC (Sec. 4.1). Each cell in the matrix denotes the distance of attended memory slots to retrieve information from, given the pair of contexts where the two object classes are present. The darker grids denote that object classes are more likely to share the same context. See Supp. for implementation details. We highlighted several context-relevant pairs of object classes from various supercategories, such as vehicles, animals, and indoor objects. For example, though

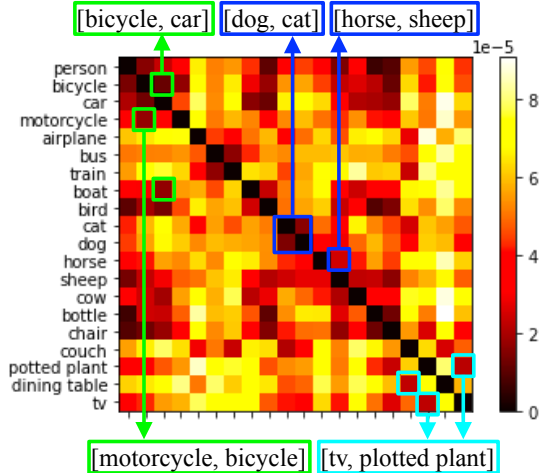


Figure 5. Pairwise KL div. of attention scores over memory slots of the external memory in SeCo for object categories in COCO-VOC. Dark grids show that targets sharing similar contexts in both categories retrieve information from similar memory slots. Colored boxes pointed by arrows denote different supercategories in VOC07, such as `vehicle`, `animal`, `indoor`.

the tv and the potted plants are not visually similar, they are contextually relevant. This suggests the external memory in SeCo learns meaningful object-context associations.

6. Discussion

We set out to determine whether and how SSL methods can capture the statistics of associations in natural images. To this end, we introduced SeCo, a simple yet effective self-supervised learning method for context reasoning, which learns object-context associations from unlabeled images. Like humans, while learning, SeCo relies on external memory to develop priors through repeated encounters with objects and their contexts, which it subsequently uses for reasoning by retrieving information from these knowledge priors. To evaluate the contextual associations learned by all models, we introduced two testing protocols, Lift-the-Flap, and Object Priming. In addition, we conducted human psychophysics experiments and introduced HOP, a human benchmark dataset for contextual reasoning. We then used it to quantitatively and qualitatively evaluate different models on the object priming task. We performed a series of ablations and analytic experiments to assess the relevance of different components of our model. Our work provides new insights into how to perform contextual reasoning via self-supervised learning.

Nevertheless, relying too much on context can be harmful in some corner cases. Incidentally, humans also suffer from this problem in multiple visual illusions, e.g., identifying elephants hoisted by airplanes. Thus, in the future, we will look into the trade-off between identifying

objects and reasoning from context. Moreover, as our proposed external memory in SeCo can bootstrap the reasoning ability, it is also worth investigating the generic memory functionality in object-centric SSL settings.

References

- [1] Adrien Bardes, Jean Ponce, and Yann Lecun. Vicreg: Variance-invariance-covariance regularization for self-supervised learning. In *ICLR 2022-10th International Conference on Learning Representations*, 2022. [2](#), [4](#), [5](#), [6](#), [7](#), [17](#)
- [2] Peter Battaglia, Razvan Pascanu, Matthew Lai, Danilo Jimenez Rezende, et al. Interaction networks for learning about objects, relations and physics. *Advances in neural information processing systems*, 29, 2016. [2](#)
- [3] Philipp Bomatter, Mengmi Zhang, Dimitar Karev, Spandan Madan, Claire Tseng, and Gabriel Kreiman. When pigs fly: Contextual reasoning in synthetic and natural scenes. In *Proceedings of the IEEE/CVF International Conference on Computer Vision*, pages 255–264, 2021. [2](#), [5](#), [7](#), [13](#)
- [4] Holger Caesar, Jasper Uijlings, and Vittorio Ferrari. Coco-stuff: Thing and stuff classes in context. In *Proceedings of the IEEE conference on computer vision and pattern recognition*, pages 1209–1218, 2018. [3](#), [5](#)
- [5] Nicolas Carion, Francisco Massa, Gabriel Synnaeve, Nicolas Usunier, Alexander Kirillov, and Sergey Zagoruyko. End-to-end object detection with transformers. In *European conference on computer vision*, pages 213–229. Springer, 2020. [2](#)
- [6] Mathilde Caron, Ishan Misra, Julien Mairal, Priya Goyal, Piotr Bojanowski, and Armand Joulin. Unsupervised learning of visual features by contrasting cluster assignments. *Advances in Neural Information Processing Systems*, 33:9912–9924, 2020. [2](#)
- [7] Mathilde Caron, Hugo Touvron, Ishan Misra, Hervé Jégou, Julien Mairal, Piotr Bojanowski, and Armand Joulin. Emerging properties in self-supervised vision transformers. In *Proceedings of the IEEE/CVF International Conference on Computer Vision*, pages 9650–9660, 2021. [2](#), [5](#), [6](#), [7](#)
- [8] Liang-Chieh Chen, George Papandreou, Iasonas Kokkinos, Kevin Murphy, and Alan L Yuille. Deeplab: Semantic image segmentation with deep convolutional nets, atrous convolution, and fully connected crfs. *IEEE transactions on pattern analysis and machine intelligence*, 40(4):834–848, 2017. [2](#)
- [9] Ting Chen, Simon Kornblith, Mohammad Norouzi, and Geoffrey Hinton. A simple framework for contrastive learning of visual representations. In *International conference on machine learning*, pages 1597–1607. PMLR, 2020. [2](#), [5](#), [6](#), [7](#)
- [10] Xiaokang Chen, Mingyu Ding, Xiaodi Wang, Ying Xin, Shentong Mo, Yunhao Wang, Shumin Han, Ping Luo, Gang Zeng, and Jingdong Wang. Context autoencoder for self-supervised representation learning. *arXiv preprint arXiv:2202.03026*, 2022. [2](#)
- [11] Xinlei Chen and Kaiming He. Exploring simple siamese representation learning. In *Proceedings of the IEEE/CVF Conference on Computer Vision and Pattern Recognition*, pages 15750–15758, 2021. [2](#), [4](#), [5](#), [6](#), [7](#)
- [12] Xinlei Chen, Li-Jia Li, Li Fei-Fei, and Abhinav Gupta. Iterative visual reasoning beyond convolutions. In *Proceedings of the IEEE conference on computer vision and pattern recognition*, pages 7239–7248, 2018. [2](#)
- [13] Wongun Choi and Silvio Savarese. A unified framework for multi-target tracking and collective activity recognition. In *European Conference on Computer Vision*, pages 215–230. Springer, 2012. [2](#)
- [14] Jia Deng, Wei Dong, Richard Socher, Li-Jia Li, Kai Li, and Li Fei-Fei. Imagenet: A large-scale hierarchical image database. In *2009 IEEE conference on computer vision and pattern recognition*, pages 248–255. Ieee, 2009. [2](#), [14](#)
- [15] Zhiwei Deng, Arash Vahdat, Hexiang Hu, and Greg Mori. Structure inference machines: Recurrent neural networks for analyzing relations in group activity recognition. In *Proceedings of the IEEE conference on computer vision and pattern recognition*, pages 4772–4781, 2016. [2](#)
- [16] Chaitanya Desai, Deva Ramanan, and Charless C Fowlkes. Discriminative models for multi-class object layout. *International journal of computer vision*, 95(1):1–12, 2011. [2](#)
- [17] Santosh K Divvala, Derek Hoiem, James H Hays, Alexei A Efros, and Martial Hebert. An empirical study of context in object detection. In *2009 IEEE Conference on computer vision and Pattern Recognition*, pages 1271–1278. IEEE, 2009. [2](#)
- [18] Alexey Dosovitskiy, Lucas Beyer, Alexander Kolesnikov, Dirk Weissenborn, Xiaohua Zhai, Thomas Unterthiner, Mostafa Dehghani, Matthias Minderer, Georg Heigold, Sylvain Gelly, et al. An image is worth 16x16 words: Transformers for image recognition at scale. In *International Conference on Learning Representations*, 2020. [2](#)
- [19] Dejan Draschkow and Melissa L-H Vö. Scene grammar shapes the way we interact with objects, strengthens memories, and speeds search. *Scientific reports*, 7(1):1–12, 2017. [3](#)
- [20] Mark Everingham, Luc Van Gool, Christopher KI Williams, John Winn, and Andrew Zisserman. The pascal visual object classes (voc) challenge. *International journal of computer vision*, 88(2):303–338, 2010. [5](#), [13](#)
- [21] Xavier Glorot and Yoshua Bengio. Understanding the difficulty of training deep feedforward neural networks. In *Proceedings of the thirteenth international conference on artificial intelligence and statistics*, pages 249–256. JMLR Workshop and Conference Proceedings, 2010. [5](#)
- [22] Josep M Gonfaus, Xavier Boix, Joost Van de Weijer, Andrew D Bagdanov, Joan Serrat, and Jordi Gonzalez. Harmony potentials for joint classification and segmentation. In *2010 IEEE computer society conference on computer vision and pattern recognition*, pages 3280–3287. IEEE, 2010. [2](#)
- [23] Priya Goyal, Piotr Dollár, Ross Girshick, Pieter Noordhuis, Lukasz Wesolowski, Aapo Kyrola, Andrew Tulloch, Yangqing Jia, and Kaiming He. Accurate, large minibatch sgd: Training imagenet in 1 hour. *arXiv preprint arXiv:1706.02677*, 2017. [5](#)

- [24] Jean-Bastien Grill, Florian Strub, Florent Althé, Corentin Tallec, Pierre Richemond, Elena Buchatskaya, Carl Doersch, Bernardo Avila Pires, Zhaohan Guo, Mohammad Gheshlaghi Azar, et al. Bootstrap your own latent—a new approach to self-supervised learning. *Advances in neural information processing systems*, 33:21271–21284, 2020. [2](#)
- [25] Kaiming He, Xinlei Chen, Saining Xie, Yanghao Li, Piotr Dollár, and Ross Girshick. Masked autoencoders are scalable vision learners. In *Proceedings of the IEEE/CVF Conference on Computer Vision and Pattern Recognition*, pages 16000–16009, 2022. [2](#)
- [26] Kaiming He, Haoqi Fan, Yuxin Wu, Saining Xie, and Ross Girshick. Momentum contrast for unsupervised visual representation learning. In *Proceedings of the IEEE/CVF conference on computer vision and pattern recognition*, pages 9729–9738, 2020. [2](#)
- [27] Kaiming He, Xiangyu Zhang, Shaoqing Ren, and Jian Sun. Deep residual learning for image recognition. In *Proceedings of the IEEE conference on computer vision and pattern recognition*, pages 770–778, 2016. [5](#), [12](#), [14](#)
- [28] R Devon Hjelm, Alex Fedorov, Samuel Lavoie-Marchildon, Karan Grewal, Phil Bachman, Adam Trischler, and Yoshua Bengio. Learning deep representations by mutual information estimation and maximization. In *International Conference on Learning Representations*, 2018. [2](#)
- [29] Derek Hoiem, Alexei A Efros, and Martial Hebert. Geometric context from a single image. In *Tenth IEEE International Conference on Computer Vision (ICCV’05) Volume 1*, volume 1, pages 654–661. IEEE, 2005. [2](#)
- [30] Hexiang Hu, Guang-Tong Zhou, Zhiwei Deng, Zicheng Liao, and Greg Mori. Learning structured inference neural networks with label relations. In *Proceedings of the IEEE Conference on Computer Vision and Pattern Recognition*, pages 2960–2968, 2016. [2](#)
- [31] Alex Krizhevsky, Ilya Sutskever, and Geoffrey E Hinton. Imagenet classification with deep convolutional neural networks. In *Advances in Neural Information Processing Systems*, volume 25, 2012. [5](#)
- [32] Lubor Ladicky, Chris Russell, Pushmeet Kohli, and Philip HS Torr. Graph cut based inference with co-occurrence statistics. In *European conference on computer vision*, pages 239–253. Springer, 2010. [2](#)
- [33] Gustav Larsson, Michael Maire, and Gregory Shakhnarovich. Learning representations for automatic colorization. In *European conference on computer vision*, pages 577–593. Springer, 2016. [2](#)
- [34] Junnan Li, Pan Zhou, Caiming Xiong, and Steven Hoi. Prototypical contrastive learning of unsupervised representations. In *International Conference on Learning Representations*, 2020. [2](#)
- [35] Dahua Lin, Sanja Fidler, and Raquel Urtasun. Holistic scene understanding for 3d object detection with rgb-d cameras. In *Proceedings of the IEEE international conference on computer vision*, pages 1417–1424, 2013. [2](#)
- [36] Tsung-Yi Lin, Michael Maire, Serge Belongie, James Hays, Pietro Perona, Deva Ramanan, Piotr Dollár, and C Lawrence Zitnick. Microsoft coco: Common objects in context. In *European conference on computer vision*, pages 740–755. Springer, 2014. [5](#)
- [37] Yong Liu, Ruiping Wang, Shiguang Shan, and Xilin Chen. Structure inference net: Object detection using scene-level context and instance-level relationships. In *Proceedings of the IEEE conference on computer vision and pattern recognition*, pages 6985–6994, 2018. [2](#)
- [38] Ilya Loshchilov and Frank Hutter. Sgdr: Stochastic gradient descent with warm restarts. *arXiv preprint arXiv:1608.03983*, 2016. [5](#)
- [39] Ishan Misra and Laurens van der Maaten. Self-supervised learning of pretext-invariant representations. In *Proceedings of the IEEE/CVF Conference on Computer Vision and Pattern Recognition*, pages 6707–6717, 2020. [2](#)
- [40] Sangwoo Mo, Hyunwoo Kang, Kihyunk Sohn, Chun-Liang Li, and Jinwoo Shin. Object-aware contrastive learning for debiased scene representation. In *35th Conference on Neural Information Processing Systems, NeurIPS 2021*. Neural Information Processing Systems, 2021. [1](#), [2](#)
- [41] Roozbeh Mottaghi, Xianjie Chen, Xiaobai Liu, Nam-Gyu Cho, Seong-Whan Lee, Sanja Fidler, Raquel Urtasun, and Alan Yuille. The role of context for object detection and semantic segmentation in the wild. In *Proceedings of the IEEE conference on computer vision and pattern recognition*, pages 891–898, 2014. [2](#)
- [42] Mehdi Noroozi and Paolo Favaro. Unsupervised learning of visual representations by solving jigsaw puzzles. In *European conference on computer vision*, pages 69–84. Springer, 2016. [2](#)
- [43] Mehdi Noroozi, Hamed Pirsiavash, and Paolo Favaro. Representation learning by learning to count. In *Proceedings of the IEEE international conference on computer vision*, pages 5898–5906, 2017. [2](#)
- [44] Deepak Pathak, Philipp Krahenbuhl, Jeff Donahue, Trevor Darrell, and Alexei A Efros. Context encoders: Feature learning by inpainting. In *Proceedings of the IEEE conference on computer vision and pattern recognition*, pages 2536–2544, 2016. [2](#), [5](#), [6](#), [7](#), [12](#), [14](#)
- [45] Maximilian Riesenhuber and Tomaso Poggio. Hierarchical models of object recognition in cortex. *Nature neuroscience*, 2(11):1019–1025, 1999. [3](#)
- [46] Rakshith Shetty, Bernt Schiele, and Mario Fritz. Not using the car to see the sidewalk—quantifying and controlling the effects of context in classification and segmentation. In *Proceedings of the IEEE/CVF Conference on Computer Vision and Pattern Recognition*, pages 8218–8226, 2019. [2](#)
- [47] Krishna Kumar Singh, Dhruv Mahajan, Kristen Grauman, Yong Jae Lee, Matt Feiszli, and Deepti Ghadiyaram. Don’t judge an object by its context: Learning to overcome contextual bias. In *Proceedings of the IEEE/CVF Conference on Computer Vision and Pattern Recognition*, pages 11070–11078, 2020. [1](#), [2](#)
- [48] Damien Teney, Lingqiao Liu, and Anton van Den Hengel. Graph-structured representations for visual question answering. In *Proceedings of the IEEE conference on computer vision and pattern recognition*, pages 1–9, 2017. [2](#)

- [49] Simon Thorpe, Denis Fize, and Catherine Marlot. Speed of processing in the human visual system. *nature*, 381(6582):520–522, 1996. [3](#)
- [50] Yuandong Tian, Xinlei Chen, and Surya Ganguli. Understanding self-supervised learning dynamics without contrastive pairs. In *International Conference on Machine Learning*, pages 10268–10278. PMLR, 2021. [2](#)
- [51] A Torralba, K Murphy, and WT Freeman. Using the forest to see the trees: Object recognition in context. *Comm. of the ACM*, 2, 2010. [2](#)
- [52] Jasper RR Uijlings, Koen EA Van De Sande, Theo Gevers, and Arnold WM Smeulders. Selective search for object recognition. *International journal of computer vision*, 104(2):154–171, 2013. [3](#), [8](#)
- [53] Ashish Vaswani, Noam Shazeer, Niki Parmar, Jakob Uszkoreit, Llion Jones, Aidan N Gomez, Łukasz Kaiser, and Illia Polosukhin. Attention is all you need. *Advances in neural information processing systems*, 30, 2017. [3](#)
- [54] Kevin Wu, Eric Wu, and Gabriel Kreiman. Learning scene gist with convolutional neural networks to improve object recognition. In *2018 52nd Annual Conference on Information Sciences and Systems (CISS)*, pages 1–6. IEEE, 2018. [2](#)
- [55] Kai Xiao, Logan Engstrom, Andrew Ilyas, and Aleksander Madry. Noise or signal: The role of image backgrounds in object recognition. In *International Conference on Learning Representations*, 2021. [3](#)
- [56] Enze Xie, Jian Ding, Wenhai Wang, Xiaohang Zhan, Hang Xu, Peize Sun, Zhenguo Li, and Ping Luo. Detco: Unsupervised contrastive learning for object detection. In *Proceedings of the IEEE/CVF International Conference on Computer Vision*, pages 8392–8401, 2021. [2](#)
- [57] Jian Yao, Sanja Fidler, and Raquel Urtasun. Describing the scene as a whole: Joint object detection, scene classification and semantic segmentation. In *2012 IEEE conference on computer vision and pattern recognition*, pages 702–709. IEEE, 2012. [2](#)
- [58] Mang Ye, Xu Zhang, Pong C Yuen, and Shih-Fu Chang. Unsupervised embedding learning via invariant and spreading instance feature. In *Proceedings of the IEEE/CVF Conference on Computer Vision and Pattern Recognition*, pages 6210–6219, 2019. [2](#)
- [59] Jure Zbontar, Li Jing, Ishan Misra, Yann LeCun, and Stéphane Deny. Barlow twins: Self-supervised learning via redundancy reduction. In *International Conference on Machine Learning*, pages 12310–12320. PMLR, 2021. [2](#)
- [60] Mengmi Zhang, Claire Tseng, and Gabriel Kreiman. Putting visual object recognition in context. In *Proceedings of the IEEE/CVF Conference on Computer Vision and Pattern Recognition*, pages 12985–12994, 2020. [2](#), [3](#), [7](#)

List of Supplementary Sections

S1 Method	13
S2 Experiments	13
S2.1 Datasets	13
S2.2 Baselines	14
S2.3 Object Priming	14
S3 Experiments, Ablation, and Memory Analysis	17
S3.1 Analysis of External Memory Size	17
S3.2 Analysis of Loss Components	17
S3.3 Probing External Memory	17

List of Supplementary Figures

S1	The architecture of Context Encoder [44] with ResNet-50 [27] as backbone encoder. Aligned with its original work, we use a channel-wise fully connected layer followed by a five-layer decoder to reconstruct the masked central region from the encoder output.	14
S2	AMT user interface for human object priming experiment. Red dots indicate the past click locations. . .	15
S3	Human priming map. The left image shows the different mouse clicks made by 3 human subjects (colored dots) for <i>cup</i> as the target object. On the right, we show the corresponding human priming map from consolidated clicks. A higher density of clicks translates to a higher probability in the priming map. See the color bar for probability values.	15
S4	SeCo priming maps highlight contextually relevant regions of the image and closely approximate human choices in the object priming task. The leftmost column shows the input image and the given target object class label used for priming. The rest of the columns from left to right are priming maps from humans, predicted by our SeCo and predicted by all baselines (Sec. 4.2). See Fig. 4 for the color bar.	16
S5	Contextual cues improve recognition of smaller target objects. We report the curves of Top 1 Accuracy on COCO-OCD versus context-object ratio in logarithmic scale.	17
S6	Analysis of external memory of SeCo. We report the top-1 accuracy for varying numbers of slots (left) and varying memory dimensionality per slot (right) in the lift-the-flap task.	18

List of Tables

S1	Ablation study on loss components. α , β , and γ are weightages of MSE loss, variance loss, and covariance loss respectively.	18
----	--	----

Algorithm 1: PyTorch-style pseudocode for SeCo

```
# Ec, Et: context and target encoders
# pc, pt: context and target projectors
# M: external memory shaped in K-by-H
# pk: key projection of external memory
# mse: mean square error loss
# var_loss: variance loss
# cov_loss: covariance loss
# alpha, beta, gamma: weightage of each loss component
#
# load a batch of N images
for x in loader:
    # randomly augmented target and context
    t, c = augment(x)

    # encode and project context, target stream
    hc, ht = Ec(x), Et(x) # N x D
    sc, st = pc(hc), pt(ht) # N x H
    # compute keys of memory
    m = pk(M) # K x H

    # retrieve memory
    p = softmax(dot(sc, m))/sqrt(H) # N x K
    sc = p * M # N x H

    # calculate loss and update
    loss = alpha * mse(sc, st) + beta * (var_loss(sc) + var_loss(st)) / 2 + gamma
        * (cov_loss(sc) + cov_loss(st))
    loss.backward()
```

S1. Method

We provide PyTorch-style pseudocode for SeCo in **Algo. 1**. In practice, we randomly sample 4 target-context pairs for each image in each iteration and average the loss value over these sampled pairs. We resize the context images to 224×224 and the target images to 96×96 .

S2. Experiments

S2.1. Datasets

To evaluate whether the learned contextual knowledge from SSL methods can generalize well in out-of-domain settings, we design two custom regimes for our experiments COCO-VOC and COCO-OCD in **Sec. 4.1**. Overlapped classes are as follows:

COCO-VOC contains the same 20 classes in hierarchy of *superclass* and subclass as defined in PASCAL VOC07 [20].

- *Person*: person
- *Animal*: bird, cat, cow, dog, horse, sheep
- *Vehicle*: aeroplane, bicycle, boat, bus, car, motorbike, train
- *Indoor*: bottle, chair, dining table, potted plant, sofa, tv/monitor

COCO-OCD contains the same 15 classes as in OCD dataset [3]: wine glass, cup, knife, bowl, apple, cake, mouse, remote, keyboard, cell phone, microwave, book, toothbrush, pillow, towel.

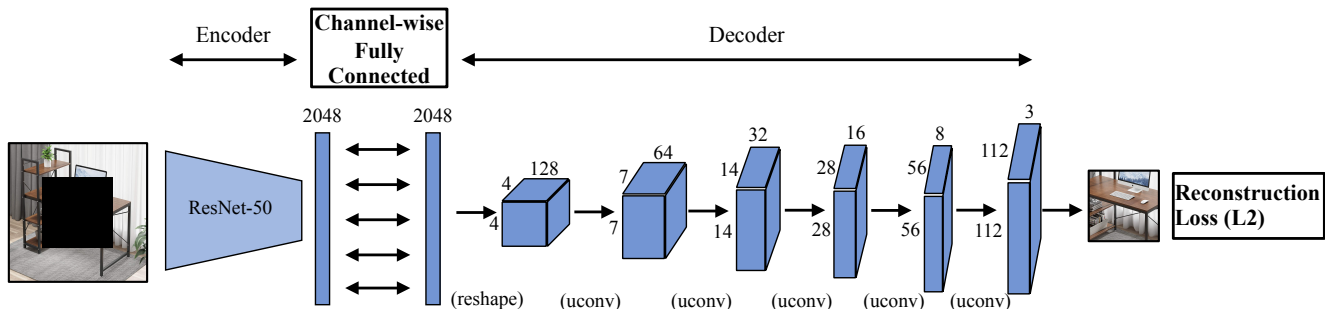


Figure S1. **The architecture of Context Encoder [44] with ResNet-50 [27] as backbone encoder.** Aligned with its original work, we use a channel-wise fully connected layer followed by a five-layer decoder to reconstruct the masked central region from the encoder output.

S2.2. Baselines

We use ResNet-50[27] as the encoder for Context Encoder [44] for fair comparisons with other works (Sec. 4.2). Following its original work, we use an asymmetric decoder with five up-convolution layers to reconstruct the masked central region. See (Fig. S1) for the architecture design. We pre-trained the model on ImageNet-1K[14] with mean square error loss for 100 epochs. We set the learning rate as 0.001. Starting from weights obtained on ImageNet-1K, we further fine-tuned the model on COCO-VOC and COCO-OCD (Sec. 4.1) respectively.

S2.3. Object Priming

[Stimulus designs] Here, we describe the steps we used to curate semantically relevant image-object pairs for the object priming experiment. First, we wanted to select images that were semantically relevant to the 15 classes of the COCO-OCD dataset (Sec. 4.1). To accomplish this, we sampled images from the test set of the COCO-OCD dataset that contained at least 3 object classes from the 15 objects classes. Next, for each image i in the sampled images, we manually select a subset C_i of semantically meaningful target classes from the 15 classes ensuring that the target class is not already present in the image. Finally, using the above steps, we ended up with 206 images and 864 unique image-object pairs.

[Human response collection] In Fig. S2, we show a screenshot of the AMT interface used for human object priming experiments. All the psychophysics experiments were conducted with the subjects' informed consent and according to the protocols approved by our Institutional Review Board. For quality controls, we only recruited participants with *master* qualification and a minimum of 95% approval rate. Each participant is compensated for participation in the experiments, which typically took 6 mins to complete.

[Post-processing] Here, we describe the post-processing of human object priming responses in detail. Specifically, we first created a 32×32 attention map by dividing the 800×800 stimuli image into 1,024 individual grids of size 25×25 . We then aggregate the clicks made in each grid such that the pixel intensity in the attention map corresponds to the number of clicks. To this 32×32 attention map, we then apply Gaussian smoothing using an 11×11 filter, followed by resizing to 224×224 , and min-max normalization to generate final human priming maps (Fig. S3).

[Model-human comparisons] We briefly introduce the process of generating priming maps for computer vision models in Sec. 4.3 and provide its pseudocode in Algo. 2. We use 5 grid sizes to generate priming maps in different scales (8×8 , 14×14 , 28×28 , 56×56 , 112×112) and normalize over these maps to obtain the final map. We provide more qualitative examples of model-human comparison in Fig. S4.



Where will you put a **apple** in this image?

Remaining Clicks: 0

Submit!

Figure S2. **AMT user interface for human object priming experiment.** Red dots indicate the past click locations.

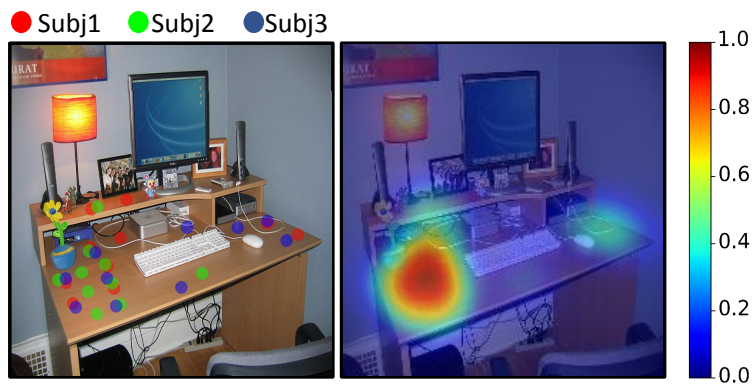


Figure S3. **Human priming map.** The left image shows the different mouse clicks made by 3 human subjects (colored dots) for *cup* as the target object. On the right, we show the corresponding human priming map from consolidated clicks. A higher density of clicks translates to a higher probability in the priming map. See the color bar for probability values.

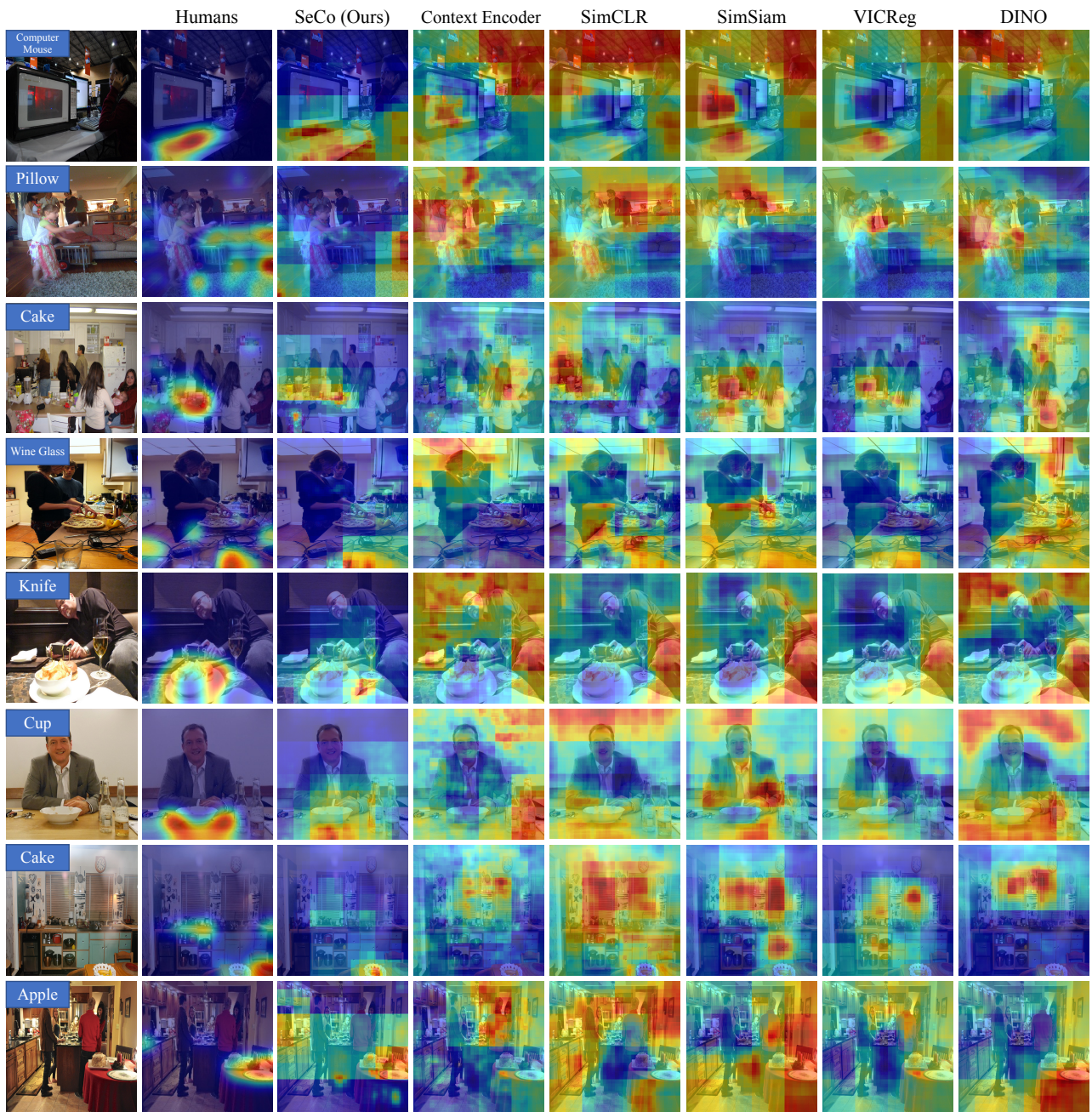


Figure S4. **SeCo priming maps highlight contextually relevant regions of the image and closely approximate human choices in the object priming task.** The leftmost column shows the input image and the given target object class label used for priming. The rest of the columns from left to right are priming maps from humans, predicted by our SeCo and predicted by all baselines (Sec. 4.2). See Fig. 4 for the color bar.

S3. Experiments, Ablation, and Memory Analysis

In **Sec. 5.1**, we incorporated contextual information into the recognition task. Specifically, for the baseline methods, we trained a linear classifier ϕ_t on the top of the frozen backbone given cropped-out objects and corresponding labels from the COCO-OCD dataset. Then, we leverage linear classifiers ϕ_c trained in the lift-the-flap task to infer from the periphery of a given object. We obtain the final prediction by multiplying the probabilities generated by ϕ_t and ϕ_c .

We break down the results according to the object sizes in **Fig. S5**. As observed, when the context-object ratio is larger than 2 in a logarithmic scale, incorporating contextual information learned with the lift-the-flap task constantly helps with recognizing smaller objects for all baselines (compare dotted line versus solid line). However, the effect of context impairs the recognition performance when the object is extremely small (the context-object ratio is less than 2). It is possible that the extremely small objects blend in the context and all recognition models fail to locate where the target objects are on the complex images.

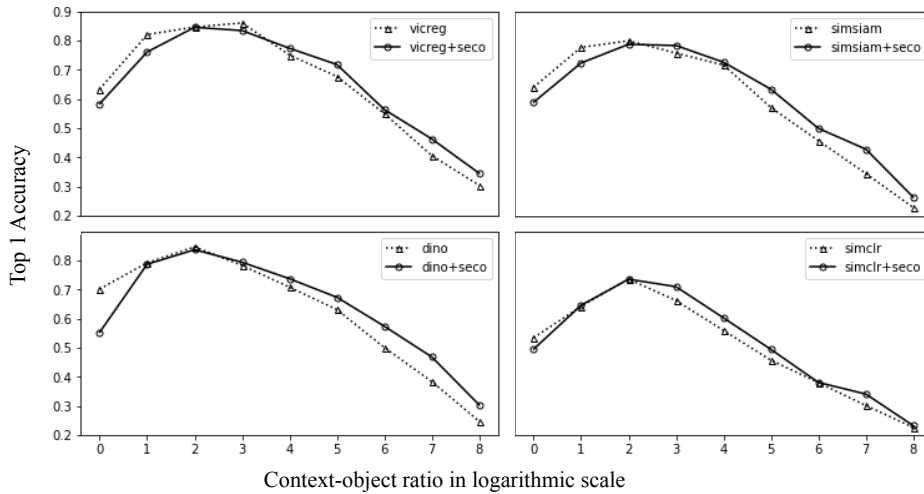


Figure S5. **Contextual cues improve recognition of smaller target objects.** We report the curves of Top 1 Accuracy on COCO-OCD versus context-object ratio in logarithmic scale.

S3.1. Analysis of External Memory Size

We also vary the number of memory slots (**Fig. S6**, left) from 100 to 800. There is a moderately positive increase of 2.5% in Top-1 accuracy in lift-the-flap. However, we observed a non-monotonic trend in Top-1 accuracy, when we vary the feature dimension of the external memory (**Fig. S6**, right). The top-1 accuracy peaks when the feature dimension equals 512. It suggests that larger memory capacity in general helps learn and store richer context-object associations; however, an overly large-sized memory may hurt context reasoning abilities, as the memory fails to generalize the learned contextual knowledge due to over-fitting.

S3.2. Analysis of Loss Components

As defined in **Sec. 3.4**, SeCo has a joint loss of MSE loss, covariance loss, and variance loss. Here, we remove each component respectively to analyze its effectiveness on pretraining. We report top-1 accuracy on COCO-OCD in **Tab. S1**. The result demonstrates that without variance loss, SeCo reached information collapse, aligning with the trend in VICReg [1]. Without covariance loss, performance drops 2% in accuracy. Different from the observations made in VICReg [1], without MSE loss, SeCo manages to achieve 41.72% in accuracy without collapses. One possible reason is that starting from weights obtained on ImageNet, the encoder has captured useful visual features. Thus, adding information regularization during pre-training on COCO-OCD can avoid collapse even without enforcing association between contexts and targets.

S3.3. Probing External Memory

In **Sec. 5.3**, we probe what the external memory has learned by visualizing the pairwise KL divergence of attention score over memory slots for object categories in COCO-VOC. Here, we provide the pseudocode of obtaining the matrix in **Algo. 3**.

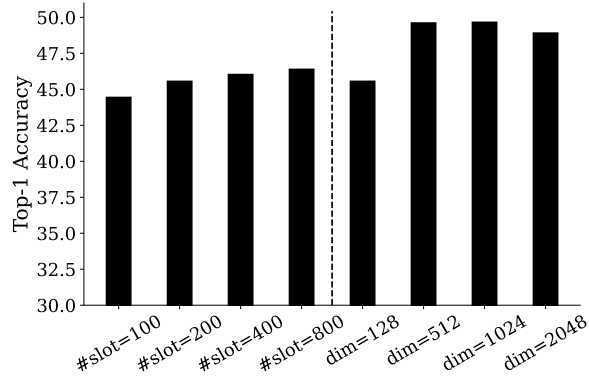


Figure S6. **Analysis of external memory of SeCo.** We report the top-1 accuracy for varying numbers of slots (left) and varying memory dimensionality per slot (right) in the lift-the-flap task.

α	β	γ	Accuracy
25	25	1	49.61
1	1	0	47.72
0	25	1	41.72
25	0	1	collapse
1	0	0	collapse

Table S1. **Ablation study on loss components.** α , β , and γ are weightages of MSE loss, variance loss, and covariance loss respectively.

Algorithm 2: PyTorch-style pseudocode for generating priming maps.

```
# Ec: trained context network with an encoder and a linear classifier
# patch-sizes: patch sizes when making erased contexts
#
# load a batch of N images
for x, label in loader:
    maps = []

    # calculate priming maps in multiple scales
    for patch_size in patch_sizes:
        # iteratively erase a patch from image
        contexts = make_context(x, patch_size)

        # retrieve probability w.r.t location for a given object category
        p = softmax(Ec(x)[:,label])

        # normalize so that priming maps in different scales can add up
        p = (p - p.min()) / (p.max() - p.min())

        # upsample to the size of input image
        patch_num = x.size[1] // patch_size
        p = p.view((patch_num,patch_num))
        p = upsample(p)
        maps.append(p)

    # finalize priming maps by averaging and normalizing over different scales
    maps = torch.stack(maps).mean(0)
    maps = (maps - maps.min()) / (maps.max() - maps.min())
```

Algorithm 3: PyTorch-style pseudocode for calculating pairwise KL divergence of attention score over memory slots for object categories in COCO-VOC.

```
# Ec: context encoders
# pc: context projector
# M: external memory shaped in K-by-H
# F: frequency matrix shaped in C-by-K
# D: pair-wise KL-divergence matrix shaped in C-by-C
# product: cartesian product of two sets
# kld: KL-divergence function
for x, label in loader:
    # obtain erased context
    c = erase(x)

    # encode and project context stream
    hc = Ec(x) # 1 x D
    sc = pc(hc) # 1 x H
    # compute keys of memory
    m = pk(M) # K x H

    # retrieve attention score over memory slots
    p = softmax(dot(sc, m))/sqrt(H) # 1 x K
    # sharpen the distribution
    top1 = p.max(0)[1]
    F[label, top1] += 1

# calculate pairwise KL-divergence
for i, j in product(range(C), range(C)):
    F[i] = (F[i] - F[i].min()) / (F[i].max() - F[i].min())
    F[j] = (F[j] - F[j].min()) / (F[j].max() - F[j].min())
    pi, pj = softmax(F[i]), softmax(F[j])
    D[i, j] = kld(pi, pj)
```
